Emirates Journal for Engineering Research

Volume 29 | Issue 3 Article 1

6-2-2024

ASSESSMENT OF AN ASSUMED STRAIN-BASED TRIANGULAR MEMBRANE ELEMENT

Abdelhak Kherfi
Laboratory of Development in Mechanics and Materials (LDMM), University of Djelfa Djelfa, Algeria, a.kherfi@univ-djelfa.dz

Kamel Zouggar
Structures and Solid Mechanical Laboratory (LMSS), Mechanical Department, Faculty of Technology Djillali Liabes University of Sidi Bel Abbes, Algeria., kamel.zouggar@dl.univ-sba.dz

Khelifa Guerraiche
Mechanical Engineering Department, Faculty of Technology, University of Batna 2, Batna, Algeria, NMISSI Laboratory, Faculty of Science and Technology, Biskra University, Biskra, Algeria., guer.khelifa@yahoo.com

Djemaa Guerraiche
Applied Energy Physics Laboratory (LPEA), Department of Physics, Faculty of Matter Sciences, University of Batna 1, Algeria., djem_ta@yahoo.fr

Antar Tahiri
Laboratory of Mechanical and Materials Development, LDMM, University of Djelfa, Djelfa, Algeria., antar.tahiri@univ-djelfa.dz

ASSESSMENT OF AN ASSUMED STRAIN-BASED TRIANGULAR MEMBRANE ELEMENT

Abdelhak Kherfi[1*], Kamel Zouggar[2], Khelifa Guerraiche[3], Djemaa Guerraiche[4], Antar Tahiri[5]

[1,] Laboratory of Development in Mechanics and Materials (LDMM), University of Djelfa, Djelfa, Algeria
a.kherfi@univ-djelfa.dz

[2] Structures and Solid Mechanical Laboratory (LMSS), Mechanical Department, Faculty of Technology Djillali Liabes University of Sidi Bel Abbes, Algeria.
zouggarkamel.zk@gmail.com

[3,] Mechanical Engineering Department, Faculty of Technology, University of Batna 2, Batna, Algeria, NMISSI Laboratory, Faculty of Science and Technology, Biskra University, Biskra, Algeria.
guer.khelifa@yahoo.com

[4,] Applied Energy Physics Laboratory (LPEA), Department of Physics, Faculty of Matter Sciences, University of Batna 1, Algeria.
djem_ta@yahoo.fr

[5,] Laboratory of Mechanical and Materials Development, LDMM, University of Djelfa, Djelfa 17000, Algeria.
antar.tahiri@univ-djelfa.dz

(Received on 30th January and Accepted on 2nd June 2024)

Abstract

This paper presents a novel triangular strain-based element designed to address plane stress and strain, axisymmetric, and dynamic problems. The proposed element has four nodes, three of which are located at the vertices and one of which is located at the midpoint of the diagonal. The corner nodes have three essential external degrees of freedom (u, v, θ), while the central node has two degrees of freedom (u, v) on one of the triangle edges. A static condensation-based treatment of the central node is employed to streamline the model and reduce computational overhead. This triangular element is applicable to both linear and dynamic analyses. Its performance is evaluated using a suite of membrane and axisymmetric problems. The obtained results demonstrate the robustness and accuracy of the proposed element.

Keywords: Strain approach, Drilling rotation, Triangular element, Linear analysis, Dynamic analysis, Axisymmetric.

Nomenclature

a_i	Constants in the displacement fields x, y, z coordinates system
w	Displacement in the z-direction [φ] displacement matrix
[D]	Elasticity matrix
[K_e]	Element stiffness matrix
D	Flexural rigidity of plate $D = Eh^3 \Big/ 2\left(1 - n^2\right)$
{δ_e}	Nodal displacement vector
L	Length of plate
ν	Poisson's ratio
$R_{1,2}$	Radius of circular plate
β_x, β_y	Rotations about y and x axes respectively
[Q]	Strain matrix
t	Thickness of plate
[C]	Transformation matrix
E	Young's modulus
Ref. Solu	Reference solution
Exact solu	Exact solution
Anal. solu	Analytical solution
SBFNT	Strain Based Four Node Triangular element
FEM	finite element method

1. INTRODUCTION

Engineering problems often find effective solutions through numerical methods such as finite elements, finite volumes, finite differences, and discrete elements methods. Among these techniques, the finite element method (FEM) holds a prominent position due to its robust mathematical foundation and versatility, making it the preferred choice for numerous applications[1], [2], [3]. Pioneering work by Turner et al.[4] introduced linear (constant-strain) triangles and bilinear rectangles within the framework of standard displacement-based elements, while Taig[5] contributed standard bilinear quadrilaterals. These elements have gained widespread adoption in two-dimensional structures, particularly for plane-stress, plane-strain, and axisymmetric-solid models. However, their propensity for excessive stiffness in scenarios dominated by linear strain gradients and their susceptibility to mesh distortions and bending issues arising from aspect ratio degradation became apparent during computational investigations.

These challenges spurred the development of improved or entirely new elements. Researchers have explored alternative strategies like hybrid stress elements[6], [7], [8], assumed strain or enhanced assumed strain elements[9], [10], [11], [12], quasi-conforming elements [13], [14], and generalized conforming elements[1], [15], [16], demonstrating their advantages over traditional finite elements. At the heart of solid mechanics research lies the pursuit of efficient and straightforward finite elements for structural analysis. One notable class of elements emerged from the strain-based approach, where displacement fields are enriched with higher-order terms without introducing additional degrees of freedom. This approach results in more accurate displacement solutions, eliminating shear locking and parasitic shear effects. Strains in this context encompass rigid body motions, constant strains, and higher-order strains.

Ashwell et al.'s approach[17], initially targeting curved structures, has been expanded to encompass plane elasticity[18], [19], [20], [21], [22]. Early work summaries are available in references[23], [24] , encompassing three-dimensional elasticity problems[10], [25], [26], [27], [28] , plate bending[10], [25], [26], [27], and shell structures[15], [29], [30], [31]. Ongoing research delves into nonlinear problems[15], [22], [32] , composite materials[25], functionally graded plates[25], [33] , and fracture mechanics[3]. These investigations have demonstrated the resilience, efficiency, and pragmatic utility of this approach in crafting robust finite elements adept at withstanding prevalent challenges like mesh sensitivity and locking problems. Significant progress has been made in applying the strain-based plane elements to solve problems on static, free and forced vibration[34], [35].

Building upon the extensive research and advancements in strain-based triangular elements, this study proposes an enhanced element with improved strain accuracy, computational efficiency, and mitigation of parasitic and shear-related issues. This element features three degrees of freedom per node (u, v, θ) for enhanced strain accuracy $\left(\varepsilon_x, \varepsilon_y, \gamma_{xy}\right)$. To further improve analysis precision and computational efficiency for plane structures, an edge central node with two degrees of freedom (u, v) is introduced. Subsequently, static

condensation [21], [22] eliminates this edge central node, resulting in a simplified three-node triangular element. Each node retains three essential translational degrees of freedom, effectively eliminating parasitic and shear-related issues while maintaining insensitivity to mesh distortions.

Through a comprehensive set of numerical experiments covering plane elasticity, axisymmetric cases, and dynamic simulations, the proposed element proves to be significantly more accurate and computationally efficient than conventional plane elements.

2. MATHEMATICAL FRAMEWORK FOR THE ELEMENT

The newly developed element, designated as SBFNT (Strain Based Four Node Triangular element), adopts a triangular shape. Each corner node possesses three degrees of freedom corresponding to two translations (u, v) and a rotation θ. Additionally, the internal node introduces two supplementary translations (*u*, *v*) (Figure 1).

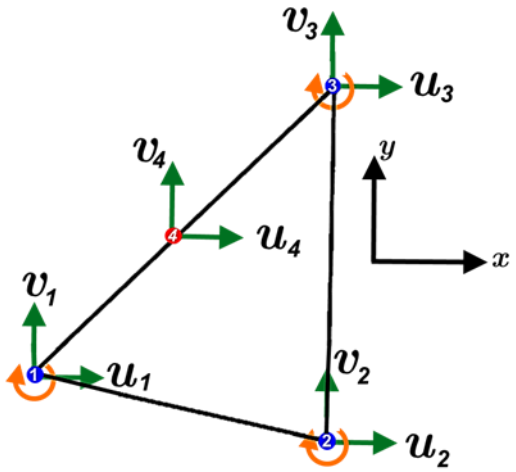

Figure 1. Strain Based Four node element (SBFNT)

For plane elasticity problems in the Cartesian coordinate system, the strain-displacement relations of the element can be expressed as:

$$\begin{cases} \varepsilon_x = \frac{\partial u}{\partial x} \\ \varepsilon_y = \frac{\partial v}{\partial y} \\ \gamma_{xy} = \frac{\partial u}{\partial y} + \frac{\partial v}{\partial x} \end{cases} \quad 1$$

$$\frac{\partial^2 \varepsilon_x}{\partial y^2} + \frac{\partial^2 \varepsilon_y}{\partial x^2} \frac{\partial^2 \gamma_{xy}}{\partial x \partial y^2} = 0 \quad 2$$

Let u and v represent the displacements along the x and y axes, respectively. The normal strains are denoted by ε_x and ε_y, while γ_{xy} represents the shear strain. The displacement field for rigid body modes is obtained by setting the three deformations in equation (1) to zero and integrating. This leads to the following expressions:

$$\begin{cases} u = a_1 - a_3 y \\ v = a_2 + a_3 x \\ \theta = a_3 \end{cases} \quad 3$$

To account for the element's drilling degree of freedom, the following equation is employed:

$$\theta = \frac{1}{2}\left(\frac{\partial v}{\partial x} - \frac{\partial u}{\partial y}\right) \quad 4$$

The SBFNT element possesses eleven independent degrees of freedom, necessitating eleven independent constants within the displacement field. As depicted in equation (3), the three constants $a_1, a_2,$ and a_3 represent the rigid body mode displacement fields. Consequently, the remaining eight constants $(a_4, a_5 \cdots a_{11})$ characterize the imposed strains of the elements, expressed as:

$$\begin{cases} \varepsilon_x = \alpha_4 + \alpha_7 y + \alpha_9 x + \alpha_{1_1} xy^2 \\ \varepsilon_y = \alpha_5 + \alpha_8 x + \alpha_{1_0} y - \alpha_{1_1} x^2 y \\ \gamma_{x_y} = \alpha_6 + \alpha_{1_1}(x^2 y - y^2 x - 2y + 2x) \end{cases} \quad 5$$

The strain functions for the current element adhere to the compatibility equation (2). They are expressed in matrix form as follows:

$$\{\varepsilon\} = [Q]\{a\} \quad 6$$

Matrix [Q] establishes the relationship between the strain fields and the unknown constants. It is defined as follows:

$$[Q] = \begin{bmatrix} 0 & 0 & 0 & 1 & 0 & 0 & y & 0 & x & 0 & xy^2 \\ 0 & 0 & 0 & 0 & 1 & 0 & 0 & x & 0 & y & -x^2 y \\ 0 & 0 & 0 & 0 & 0 & 1 & 0 & 0 & 0 & 0 & x^2 y - y^2 x - 2y + 2x \end{bmatrix} \quad 7$$

By performing the integration of equations (5) and utilizing equations (3) as substitutions, we arrive at the final displacement functions

$$\begin{cases} u = \alpha_1 - \alpha_3 y + \alpha_4 x + \frac{1}{2}\alpha_6 y + \alpha_7 xy - \frac{1}{2}\alpha_8 y^2 + \frac{1}{2}x^2\alpha_9 + \alpha_{11}\left(\frac{x^2y^2}{2} - y^2\right) \\ v = \alpha_2 + \alpha_3 x + \alpha_5 y + \frac{1}{2}\alpha_6 x - \frac{1}{2}\alpha_7 x^2 + \alpha_8 xy + \frac{1}{2}\alpha_{10} y^2 + \alpha_{11}\left(x^2 - \frac{x^2y^2}{2}\right) \\ \theta = \alpha_3 - \alpha_7 x + \alpha_8 y + \alpha_{11}\left(x + y - \frac{xy^2}{2} - \frac{x^2 y}{2}\right) \end{cases} \quad 8$$

The aforementioned relationships can be represented in matrix form as follows:

$$\{u\} = [T]\{a\} \quad 9$$

For which the matrix [T] takes the following form:

$$[T] = \begin{pmatrix} [P] \\ [R] \end{pmatrix} \quad 10$$

The constituent matrices [P] and [R] are defined as follows:

$$[P] = \begin{bmatrix} 1 & 0 & -y & x & 0 & \frac{y}{2} & xy & \frac{-y^2}{2} & \frac{x^2}{2} & 0 & \frac{x^2y^2}{2} - y^2 \\ 0 & 1 & x & 0 & y & \frac{x}{2} & -\frac{x^2}{2} & xy & 0 & \frac{y^2}{2} & x^2 - \frac{x^2y^2}{2} \end{bmatrix} \quad 11$$

$$[R] = \begin{bmatrix} 0 & 0 & 1 & 0 & 0 & 0 & -x & y & 0 & 0 & x + y - (\frac{xy^2}{2} - \frac{x^2y}{2}) \end{bmatrix} \quad 12$$

The displacements at the nodes and the coefficients in the vector {a} are related by:

$$\{q_e\} = [C]\{a\} \quad 13$$

where:

$$\{q_e\} = \{u_1 \quad v_1 \quad \theta_1 \quad u_2 \quad v_2 \quad \theta_2 \quad u_3 \quad v_3 \quad \theta_3 \quad u_4 \quad v_4\}^T \quad 14$$

$$\{a\} = \{a_1 \quad a_2 \quad a_3 \quad a_4 \quad a_5 \quad a_6 \quad a_7 \quad a_8 \quad a_9 \quad a_{10} \quad a_{11}\}^T \quad 15$$

In addition, the 11x11 matrix [C] acts as a mathematical representation of the structural relationships between the coefficients (a_1 to a_{11}) and the resulting nodal displacements. This mapping is expressed as follows:

$$[C] = \begin{pmatrix} P(x_1, y_1) \\ R(x_1, y_1) \\ P(x_2, y_2) \\ R(x_2, y_2) \\ P(x_3, y_3) \\ R(x_3, y_3) \\ P(x_4, y_4) \end{pmatrix} \quad 16$$

Based on equation (13), we can deduce:

$$\{a\} = [C]^{-1}\{q_e\} \quad 17$$

Substituting equation (17) into equations (6) and (9) yields:

$$\{U\} = [P][C]^{-1}\{q_e\} = [N]\{q_e\} \quad 18$$

and

$$\{\varepsilon\} = [Q][C]^{-1}\{q_e\} = [B]\{q_e\} \quad 19$$

where:

$$\begin{cases} [N] = [P][C]^{-1} \\ [B] = [Q][C]^{-1} \end{cases} \quad 20$$

where: [N] and [B] represent respectively the shape functions and the matrix that link deformation to nodal displacement $\{q_e\}$

The mathematical representation of stress and strain is:

$$\{\sigma\} = [D]\{\varepsilon\} \quad 21$$

Where [D] represents the elasticity matrix for plane stress and plane strain, as defined in Appendix A. To derive the element stiffness matrix, the following steps are involved:

The weak form, which is given in the following equation:

$$\int_{Ve} \delta\{\varepsilon\}^T\{\sigma\}dV = \int_{Ve} \delta\{U\}^T\{f_v\}dV \quad 22$$

Substituting the values from equations (18), (19), and (21) into equations (22) results in:

$$\delta\{q_e\}^T\left(\int_{Ve}[B]^T[D][B]dV\right)\{q_e\} = \delta\{q_e\}^T\left(\int_{Ve}[N]^T\{f_V\}dV\right) \quad 23$$

where:

$$[K_e] = \int_{Ve}[B]^T[D][B]dV \quad 24$$

$$[K_e] = t[C]^{-T}(\iint[Q]^T[D][Q]dxdy)[C]^{-1} \quad 25$$

With 't' denoting the thickness

$$[K_e] = t[C]^{-T}[K_0][C]^{-1} \quad 26$$

The juxtaposition of equations (25) and (26) leads to

$$[K_0] = \iint[Q]^T[D][Q]dxdy \quad 27$$

Through the application of numerical integration techniques:

$$[K_0] = \int_{-1}^{+1}\int_{-1}^{+1}[Q]^T[D][Q]det|J|d\xi\, d\eta \quad 28$$

Where [J] denotes the Jacobian matrix and the element nodal body forces vector is given by:

$$\{F_b\} = \int_{Ve}[N]^T\{f_v\}\,dV = [C]^{-T}\left(\int_{Ve}[P]^T\{f_v\}\,dV\right) \quad 29$$

Once all the elements have been assembled, the overall stiffness [K] is fed into the static equations as follows:

$$[K]\{q\} = \{F\} \quad 30$$

2.1 Case of Axisymmetric

Under the assumption of axisymmetric conditions, the strain components are expressed as:

$$\begin{cases} \varepsilon_r = \frac{\partial u}{\partial r} \\ \varepsilon_z = \frac{\partial v}{\partial z} \\ \gamma_{rz} = \frac{\partial u}{\partial z} + \frac{\partial v}{\partial r} \\ \varepsilon_\theta = \frac{u}{r} \end{cases} \quad 31$$

In the context of axisymmetric analysis, the element stiffness matrix takes the following form:

$$[K_e] = \int_{Ve}[B]^T[D][B]rdV \quad 32$$

The radial coordinate is denoted by 'r', and the axisymmetric elasticity matrix is represented by [D],

as detailed in Appendix A. It is important to note that our numerical integration employs the Gauss quadrature technique. Moreover, in instances of forced vibration, the complex response method is utilized, as described in[36] .

3. NUMERICAL VALIDATION

This section presents a comprehensive evaluation of the element's accuracy under various analysis types, including plane strain, plane stress, axisymmetric, and dynamic. The performance of the proposed element is benchmarked against the following established elements:

SBQM[19]	5-node quadrilateral element with in-plane rotation based on the strain approach
Q4	Standard four-nodes quadrilateral element.
Q8	Standard eight-nodes quadrilateral element.
Q6[20]	Quadrilateral element with six nodes.
FRQ[9]	4-node quadrilateral element based on the "Plane Fiber Rotation" concept
CST[37]	Constant strain triangle CST-3/6C
LST[38]	Linear Strain Triangle
CST Hybrid[37]	Cook's plane hybrid triangle
SBT3[38]	An assumed strain based on triangular element with drilling rotation
CPS8[19]	Classic 8-node quadrilateral element in-plane stress with exact integration (Abaqus).
SBRIEIR [39]	Element with strain field at four nodes with in-plane rotation.
Q4CST[20]	The constant strain quadrilateral.
QM5[20]	Plane stress element and Verbeke plate element boundary element formulation.
SBQ5 [40]	Strain-based quadrilateral element with five nodes.
SBE[41]	Strain Based Element
CQUAD4[42]	MSC/NASTRAN
SBTDR[43]	Strain-based triangular element

3.1 PLANE LINEAR ELASTICITY TESTS

3.1.1. MCNEAL'S BEAM

The susceptibility of the proposed element to mesh distortion is assessed using the McNeal beam depicted in Figure 2. Three distinct meshes, namely rectangular, parallelogram, and trapezoidal, are employed. The McNeal and Harder[44] test, widely recognized as the benchmark for evaluating mesh distortion sensitivity, is utilized. Two loading scenarios are considered: pure bending and transverse linear bending. The pertinent mechanical and geometrical parameters are presented in Figure 2. Table 1 summarizes the results obtained by the proposed element compared to other elements.

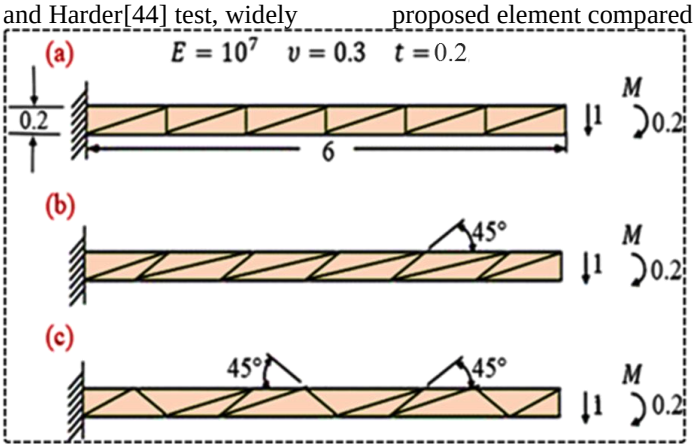

Figure 2. McNeal's cantilever beam (a) rectangular (b) trapezoidal (c) parallelogram

Table 1. Normalized deflection at the tip of the McNeal's beam

	LOAD P			**LOAD M**		
	MESH TYPE			**MESH TYPE**		
ELEMENT	**Rectangular (a)**	**Parallelogram (b)**	**Trapezoidal (c)**	**Rectangular (a)**	**Parallelogram (b)**	**Parallelogram (c)**
SBQM[19]	0.993	0.964	0.972	1.00	1.00	1.00
Q4	0.093	0.035	0.003	0.093	0.031	0.022
Q8	0.951	0.919	0.854	1.00	0.994	0.939

SBT3[38]	0.964	0.950	0.950	0.989	0.988	0.988
SST[37]	0.994	0.943	0.921	1	1	1
SBE[41]	1.00	0.976	0.978	1.00	0.989	0.989
SBTDR[43]	0.992	0.904	0.888	1.00	1.00	1.00
SBFNT	**0.993**	**0.880**	**0.930**	**1.00**	**1.00**	**1.00**
Ref. Solu[44]	**- 0.1081**			**− 0.0054**		

The strain-based elements SBFNT, SBQM, SBTDR and SBE, along with the standard eight-node quadrilateral element Q8, exhibit low sensitivity to mesh distortion under both loading cases in trapezoidal and parallelogram meshes. Specifically, SBQM and SBE outperform slightly SBFNT in shear testing due to their quadrilateral shape.

The SBFNT element demonstrates negligible sensitivity across all mesh types, outperforming other elements in terms of accuracy, particularly in flexion in cases (b) and (c). However, the transverse shear locking propensity of the standard four-node quadrilateral element Q4, arising from its excessive rigidity, adversely affects its results. After statically condensing the central edge node, resulting in a simplified triangular element with three nodes, the SBFNT (Strain Based Four Node Triangular element) element offers significant computational advantages. Its straightforward structure enhances both time efficiency and cost-effectiveness in computational analyses.

3.1.2. BEAM IN-PLANE BENDING

To validate the developed element's performance in the context of the cantilever beam problem subjected to a uniform vertical load, as illustrated in Figure 3, references[9], [18] were consulted. The vertical displacement at the beam's free end is computed using five meshes depicted in Figure 3.

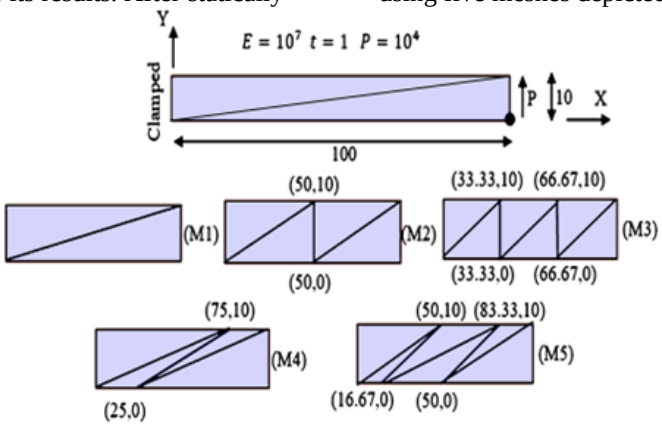

Figure 3. Visualization of data and meshes for beam in-plane bending analysis

For reference purposes, Timoshenko's beam theory was implemented:

$$V_c^{ref} = \frac{PL^3}{3EI} + \frac{6P_zL}{5GA} \quad 33$$

Table 2 presents the results obtained by the SBFNT element for various meshes (M1, M2, M3, M4, and M5). These results are compared against those reported in the literature for selected membrane elements, revealing the following observations:

- The SBFNT element consistently outperforms the Q4, FRQ, and SBRIEIR elements in terms of accuracy.
- For regular meshes (M1, M2, and M3), the SBFNT element demonstrates comparable results to the SBT3, LST, and Q8 elements.
- In the presence of distorted meshes (M4 and M5), the SBFNT element exhibits superior insensitivity compared to other membrane elements.

Table 2. Vertical displacement of a beam in plane

Mesh Type	FRQ[9]	Q4 [18]	Q8[18]	LST[38]	CST[38]	SBT3[38]	SBRIEIR[19]	SBQM[19]	SBFNT
M1	2.76	0.10	3.03	3.00	0.05	2.88	2.86	3.02	3.03
M2	3.44	0.38	3.7	370	0.13	2.90	3.57	3.77	3.77
M3	3.56	0.75	3.84	3.84	0.25	2.93	3.71	3.91	3.91
M4	1.09	0.12	0.64	3.02	0.06	2.92	2.92	3.04	3.047
M5	1.61	0.22	1.76	3.09	0.10	2.97	3.04	3.14	3.13
Ref. Solu[18]			**4.03**						

3.1.3. COOK'S SKEW BEAM

The Cook's skew beam, depicted in Figure 4, is a widely recognized benchmark problem for assessing the performance of planar elements. Numerous researchers have investigated this problem, as documented in[45], [46], [47] . Due to the absence of an analytical solution, the reference solution is obtained using ABAQUS's CPS8 element with a refined 64×64 mesh. The mechanical properties, geometrical dimensions, and loading conditions for the analyzed structure are presented in Figure 4. The results for the vertical deflection at point C are summarized in Table 3.

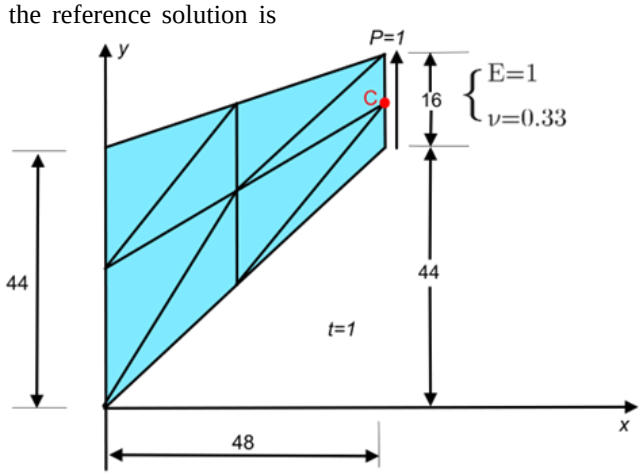

Figure 4. Cook's skew beam

The SBFNT element demonstrates satisfactory agreement with the reference solution, even with a relatively coarse mesh compared to the Q4, SSQUAD[24], CQUAD4[42], SBQM [19], CPS8[19] and SBTDR[43] elements. This observation underscores the SBFNT element's robustness and efficiency in handling complex stress distributions.

Table 3. Tip vertical deflection of the Cook's skew beam

	Vertical displacement at point C			
	Mesh			
Element	**2×2**	**4×4**	**8×8**	**16×16**
Q4	11.80	18.29	22.08	23.43
SSQUAD[16]	25.65	24.27	24.01	23.96
CQUAD4[42]	21.05	23.02	23.69	23.94
SBQM[19]	23.2173	23.4350	23.7376	23.9817
CPS8[19]	23.35	24.54	23.8793	23.8596
CSTHybrid[37]	19.41	22.17	23.37	23.77
SST[37]	20.94	23.84	24.18	24.13
SBTDR[43]	15.85	20.96	25.55	-
SBFNT	**22.31**	**23.92**	**23.98**	**23.98**
Ref. Solu[36]	**23.96**			

3.1.4 THICK-WALLED CYLINDER UNDER INTERNAL PRESSURE

To assess the performance of the proposed element in handling variable material properties (a variable Poisson's ratio), a thick-walled cylinder subjected to uniform internal pressure is analyzed. The problem is considered under plane strain conditions. Due to symmetry, only one-quarter of the cylinder is modeled. The mechanical properties and geometrical dimensions are depicted in Figure 5. The results for the radial displacement at the inner radius are presented in Table 4. The reference solution is obtained from[48]:

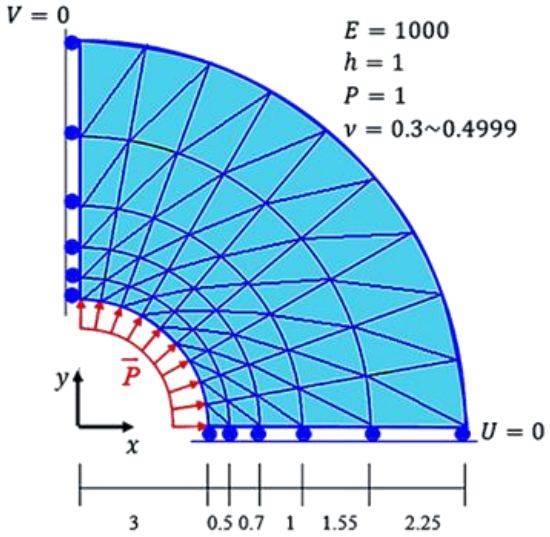

Figure 5. Thick-walled cylinder under internal pressure

Table 4. Normalized radial displacements at the inner radius of the thick-walled cylinder

Poisson's ratio	Q4[46]	SBQM[19]	Q8	SBQ5[40]	SBRIEIR[19]	**SBFNT**	**Ref. Solu**[48]
0.3	0.986	0,9869	1.184	0.990	0.9698	**0.952**	**4.5825**
0.49	0.845	0,9784	1.108	1.009	0.8532	**0.956**	**5.0399**
0.499	0.398	0,9770	1.037	1.011	0.5200	**0.956**	**5.0602**
0.4999	0.053	0,9768	1.036	1.011	0.1539	**0.956**	**5.0623**

The normalized radial displacement results presented in Table 4 demonstrate that the Q8 elements and the strain-based elements SBFNT, SBQM, SBQ5, and SBRIEIR are insensitive to locking caused by the variation of Poisson's ratio. Notably, the triangular element SBFNT exhibits less accuracy than the quadrilateral ones. Triangular elements like SBFNT excel in accommodating curved shapes, whereas rectangular elements are more suitable for straightforward designs.

3.1.5 THIN CIRCULAR CONSOLE BEAM UNDER SHEAR LOADING

To assess the performance of the SBFNT element in analyzing thin, curved beams, three meshes (6×1, 12×2, and 24×4) were employed. The geometrical dimensions, loading, and boundary conditions are as specified in[47] and depicted in Figure 6.

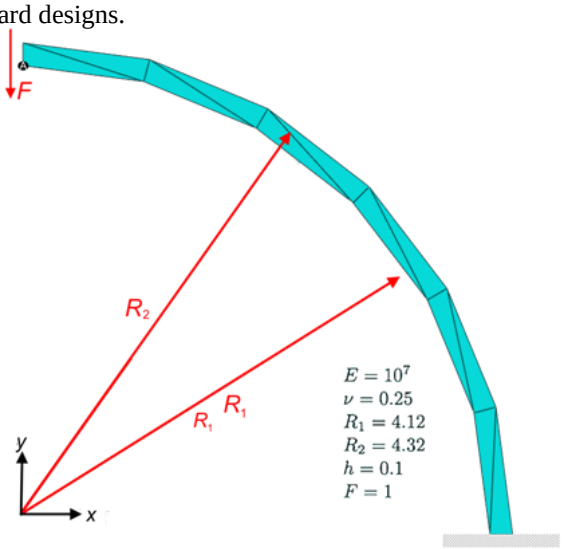

Figure 6. Thin circular console beam modelled with (6×1) quadrilateral elements

The SBFNT element's normalized vertical displacements at a specific point are compared to those of other elements in Table 5. It is evident that the SBFNT element's displacement rapidly converges towards the reference solution and outperforms the CPS4, SBTDR, SST, and SBRIEIR elements. Moreover, its results closely match those of the CPS8 element.

Table 5. Normalized vertical displacement at point A of a thin circular console beam

Mesh	CPS4[47]	CPS8[47]	SBTDR[43]	SST[37]	SBRIEIR[19]	**SBFNT**
6×1	0.073	0.881	0.073	0.02536	0.504	**0.726**
12×2	0.247	1.006	0.464	0.09599	0.797	**0.878**
24×4	0.572	1.013	0.797	0.28189	0.936	**0.970**
Ref. Solu[47]			**-0.08734**			

3.2 AXISYMMETRIC ELASTICITY TEST

3.2.1 POINT LOADED CIRCULAR PLATE BENDING

For the analysis an anisotropic simply supported circular plate with a thickness of h = 1 and a radius of r = 10 is subjected to a point load of P = 10 at the center, as illustrated in Figure 7. The analytical solution for this problem is derived from Timoshenko's work[49].

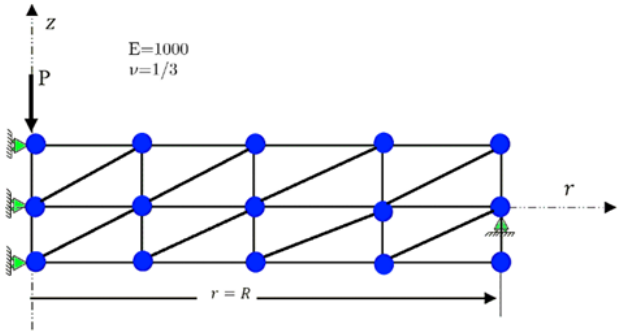

Figure 7. Geometry and mesh of a simply supported circular plate under a concentrated load.

The analytical formulas for the bending moments and the resulting stresses are provided as follows:

$$\begin{cases} M_{rr} = \frac{P}{4\pi}(1+\upsilon)\ln\left(\frac{b}{a}\right) \\ M_{\theta\theta} = \frac{P}{4\pi}((1+\upsilon)\ln\left(\frac{b}{a}\right)+1-\upsilon) \end{cases} \quad 34$$

$$\begin{cases} \sigma_{rr} = \frac{12M_{rr}z}{h^3} \\ \sigma_{\theta\theta} = \frac{12M_{\theta\theta}z}{h^3} \end{cases} \quad 35$$

where 'a' and 'b' denote the internal and external radii of the plate subjected to a concentrated load, respectively.

As the internal radius 'a' approach zero, the bending moments and stresses expressed in equations (20) and (21) diverge to infinity. To facilitate comparisons between analytical and numerical solutions, the analytical values of the internal radius a will be selected very close to zero ($r \leq \ r_{struc} = r/1000$).The stresses on the bottom and top surfaces of the plate are:

$$\begin{cases} \sigma_{rr} = \pm\frac{12M_{rr}(h/2)}{h^3} = \pm 6M_{rr}/h^2 \\ \sigma_{\theta\theta} = \pm\frac{12M_{\theta\theta}(h/2)}{h^3} = \pm 6M_{\theta\theta}/h^2 \end{cases} \quad 36$$

At a specific radius 'r', the precise radial displacement is determined as follows:

$$\begin{cases} u_r = -z\cdot\frac{\delta u_z}{\delta r} = \frac{P}{S\cdot\pi\cdot D}\left[\frac{3+\upsilon}{1+\upsilon} - (1+2\cdot\log\left(\frac{b}{a}\right))\right]\times r\cdot z \\ u_z = \frac{P}{16\cdot\pi\cdot D}\left[\frac{3+\upsilon}{1+\upsilon}(a^2-b^2)+2\cdot r^2\log\left[\frac{b}{a}\right)\right] \end{cases}$$

37

And where:

$$D = \frac{Eh^3}{12\cdot(1-2\upsilon)} \quad 38$$

As illustrated in Figures 8, 9, and 10, the vertical displacements predicted by the SBFNT and Q8 elements closely match the theoretical solution. For a coarse mesh, the Q4 element produces results that deviate significantly from the analytical solution due to the shear locking issue arising from its excessive rigidity. Although refining the mesh improves the accuracy of the Q4 element's results, they still fall short of those obtained with the SBFNT and Q8 elements. Regarding the radial and hoop stresses, the developed elements provide consistently accurate results even with a coarse mesh, in contrast to the Q4 element, which yields erroneous results.

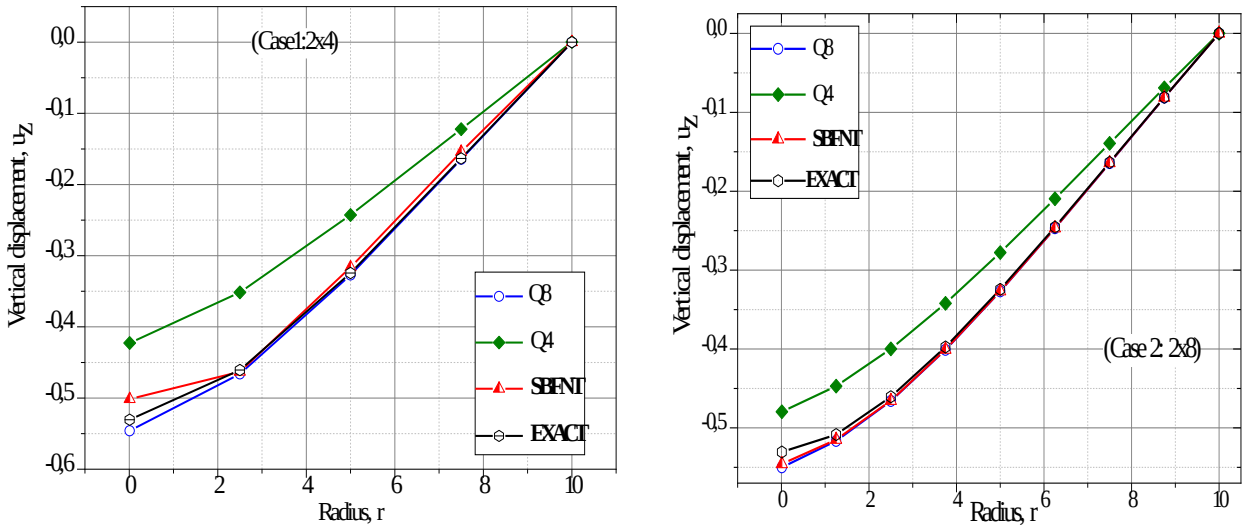

Figure 8. Displacement distribution along the line $z = \frac{h}{2}$

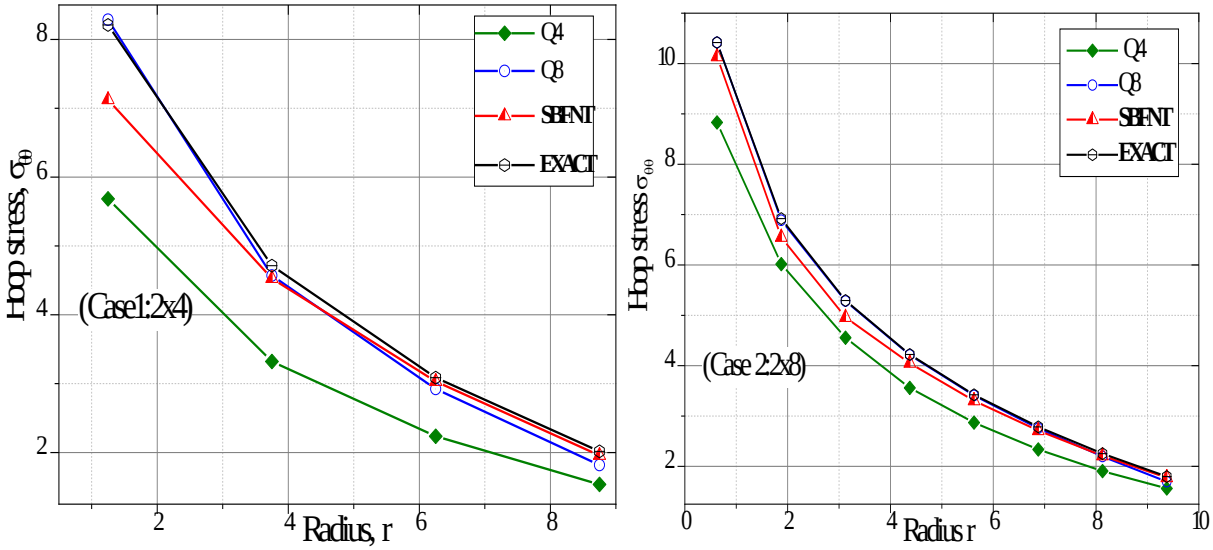

Figure 9. Point Loaded Circular Plate Bending (Hoop stress $\sigma_{\theta\theta}$ calculated at the center of the elements).

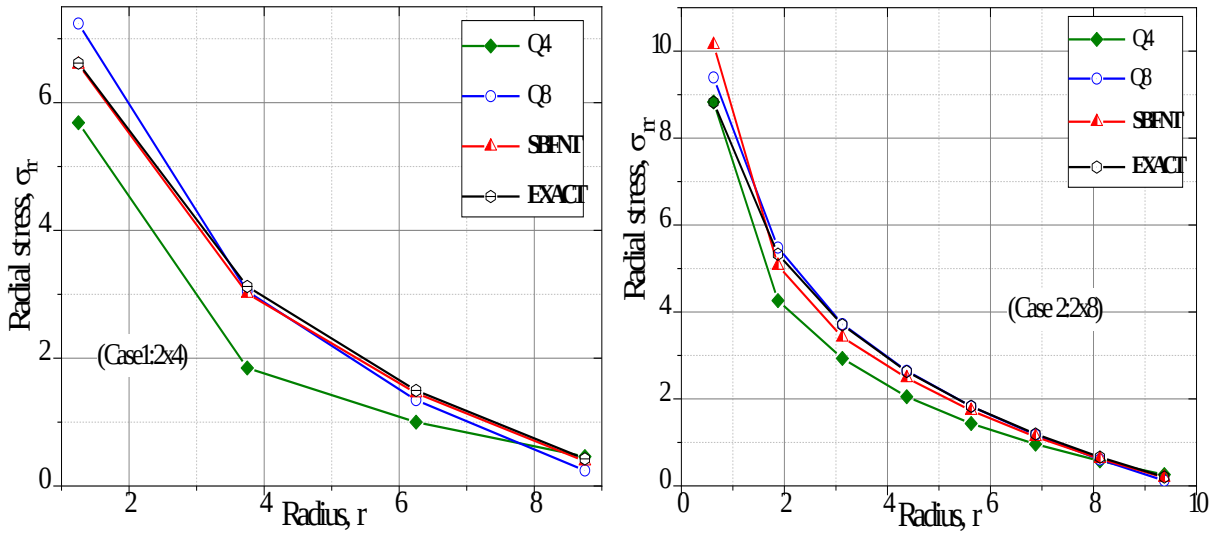

Figure 10. Point Loaded Circular Plate Bending (Radial stress σ_{rr} calculated at the center of the elements).

3.2.2 SIMPLY SUPPORTED CIRCULAR PLATE UNIFORMLY LOADED

A simply supported circular plate subjected to a uniform load is analyzed, assuming a plate thickness of *t=1*. Two distinct meshes were employed to discretize the plate. The first mesh is a rectangular mesh with a distortion factor of *e=0*, while the second is a trapezoidal mesh with a distortion factor of *e=0.025*, as depicted in Figure 11. The reference solution for this problem is adopted from[49].

$$w(r) = \frac{P \cdot {r_0}^4}{64 \cdot D(1+\upsilon)} \left[2 \cdot (3+\upsilon) \cdot \left(1 - \left(\frac{r}{r_0}\right)^2\right) - (1+\upsilon) \cdot \left(1 - \left(\frac{r}{r_0}\right)^4\right) \right] \quad (39)$$

$$\begin{cases} w_{max} = w(0) \\ w_{max} = \frac{P \cdot {r_0}^4 (5+\upsilon)}{64 \cdot D \cdot (1+\upsilon)} \end{cases} \quad (40)$$

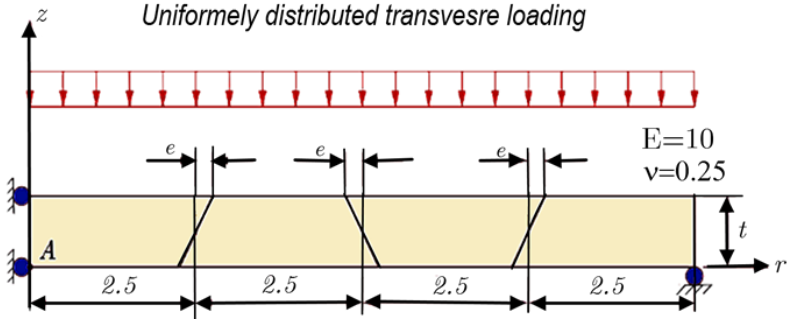

Figure 11. Simply supported uniformly loaded circular plate

Table 6. Normalized vertical displacement at the center 'A' for the uniformly loaded circular plate

	u_{zA}	
	Mesh type	
Element	**Rectangular**	**Trapezoidal**
Q4	0.696	0.694
Q8	1.0079	1.0183
SBFNT	**0.993**	**0.993**
Ref. sol[49]	**−738.280**	

The displacement results presented in Table 6 demonstrate that the SBFNT element accurately approximates the exact solution, closely matching the performance of the Q8 element. In contrast, the Q4 element yields inferior results. The SBFNT element excels in scenarios where bending is the predominant stress state.

3.2.3 INTERNALLY PRESSURIZED THICK CYLINDER

Consider an infinitely long thick cylinder with radius 'r' subjected to internal pressure. The material properties, boundary conditions, and loading conditions applied to the model are depicted in Figure 12. The problem is analyzed under plane strain conditions. Two meshes (1×4 and 1×8) comprising axisymmetric quadrilateral elements are employed to discretize a *d=2* 'slice' of the thickness, as shown in the same figure. The analytical solution for a thick cylinder subjected to internal pressure, as proposed by Timoshenko (Goodier, 1951), is given by:

$$\begin{cases} \sigma_{rr} = \frac{Pa^2}{b^2-a^2}\left(1 - \frac{b^2}{r^2}\right) \\ \sigma_{zz} = \frac{2Pa^2\upsilon}{b^2-a^2} \\ \sigma_{\theta\theta} = \frac{Pa^2}{b^2-a^2}\left(1 + \frac{b^2}{r^2}\right) \end{cases} \quad (41)$$

For a given radius r, the exact radial displacement is:

$$U_{rr} = \frac{a^2(1+\nu)}{E} \times \left(\frac{b^2 + r^2(1-2\nu)}{(b^2-a^2) \cdot r}\right) \quad (42)$$

Stress and displacement results obtained for the formulated elements and those for elements Q4 and Q8 are presented in Figures 13, 14, and 15. The numerical results show good agreement with the analytical solution for all elements, with stress results calculated at the element centers.

For a coarse mesh size of (1×4), the SBFNT and Q8 elements exhibit excellent accuracy. Element Q4 demonstrates improved accuracy with mesh refinement (1×8), particularly for radial displacement. This improvement is attributed to the low-stress gradients observed in this case, which differ from those in the axisymmetric cylindrical shell scenario.

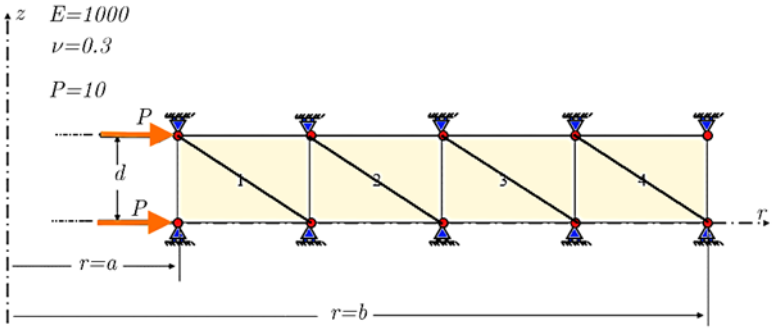

Figure 12. Geometry and mesh of a thick cylinder subjected to internal pressure

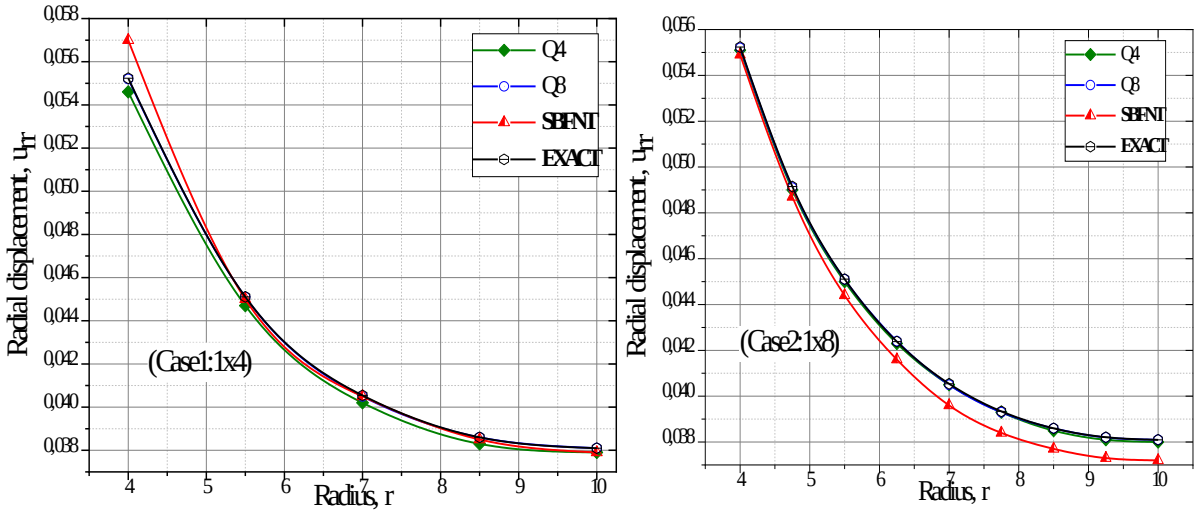

Figure 13. Displacement distribution along the line (z=0)

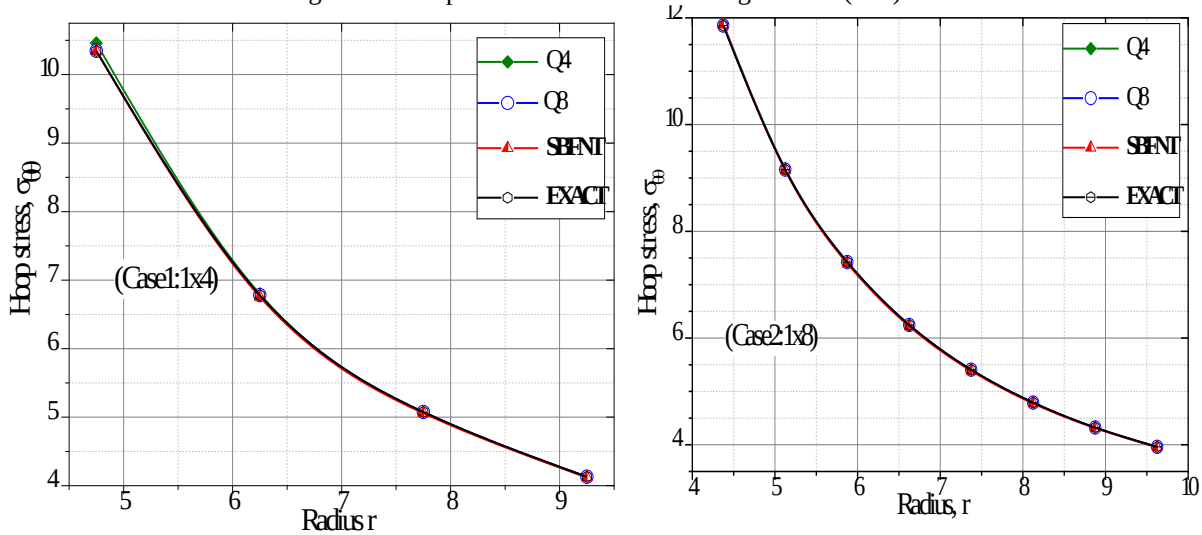

Figure 14. Hoop stress distribution at the center of elements

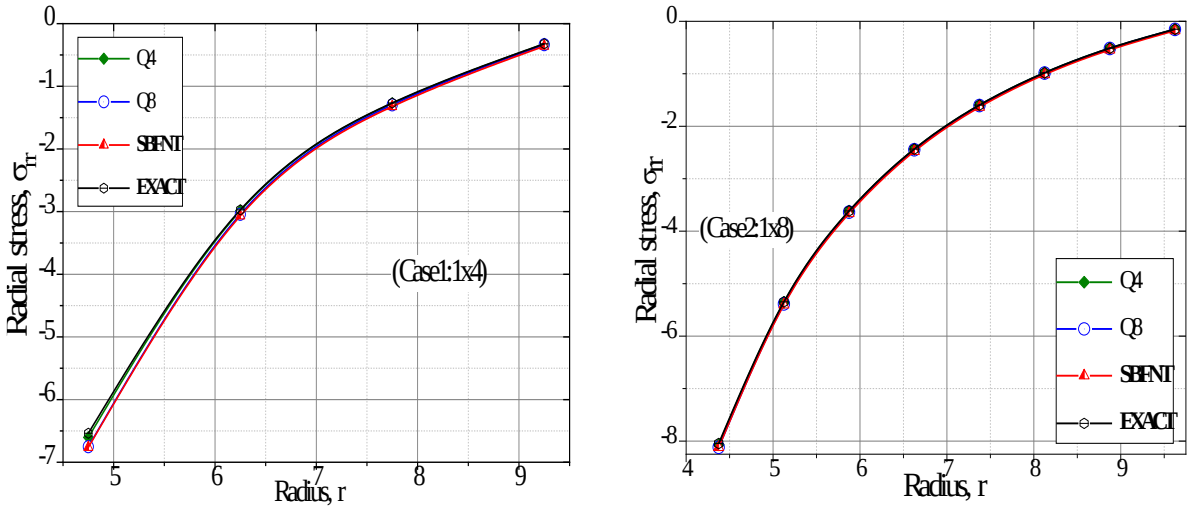

Figure 15. Radial stress distribution at the center of elements

3.2.4 AXISYMMETRIC CYLINDRICAL SHELL

A thin cylindrical shell with a radius-to-thickness ratio $R/e = 168$ is subjected to an end moment[20], as illustrated in Figure 16. This problem represents an example of a thin shell with axisymmetric loading, for which an exact solution can be obtained using shell theory in the case of infinite length. A quadrilateral element is employed through the thickness of the shell. The theoretical solution for shells[49] is used as a benchmark to compare the numerical radial displacements for both the proposed element and various other element types. The results are presented in Table 7 and Figure 17. The proposed element exhibits excellent accuracy, which becomes even more evident in bending-dominated scenarios.

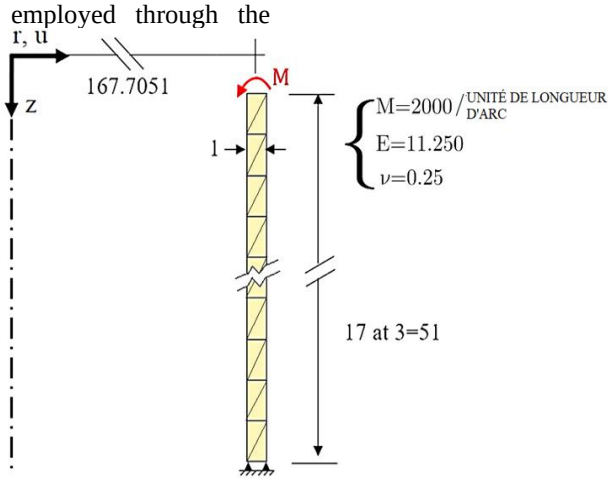

Figure 16. Cylindrical shell analysis.

Table 7. Radial displacements (u) for the axisymmetric cylindrical shell.

	Radial Displacements u					
Z	Q4CST[20]	QM5[20]	Q4[20]	Q6[20]	**SBFNT**	**Anal. Solu**[20]
0	39.97	98.56	46.47	100.01	**99.9312**	**100.00**
3	26.04	47.87	29.17	48.98	**48.9355**	**48.88**
6	14.98	13.49	15.69	14.19	**14.3776**	**14.31**
9	6.56	-7.29	5.69	-6.54	**-6.5302**	**-6.57**
12	0.47	-17.77	-1.31	-17.15	**-17.1453**	**-17.16**
15	-3.65	-21.17	-5.82	-20.70	**-20.6865**	**-20.68**
18	-6.16	-20.21	-8.35	-19.88	**-19.8693**	**-19.85**
21	-7.40	-16.97	-9.39	-16.83	**-16.7709**	**-16.75**

24	-7.68	-12.92	-9.33	-12.85	**-12.8413**	**-12.82**
27	-7.27	-8.98	-8.55	-9.00	**-8.9934**	**-8.95**
30	-6.40	-5.65	-7.32	-5.72	**-5.7233**	**-5.63**
33	-5.27	-3.12	-5.87	-3.23	**-3.2319**	**-3.06**

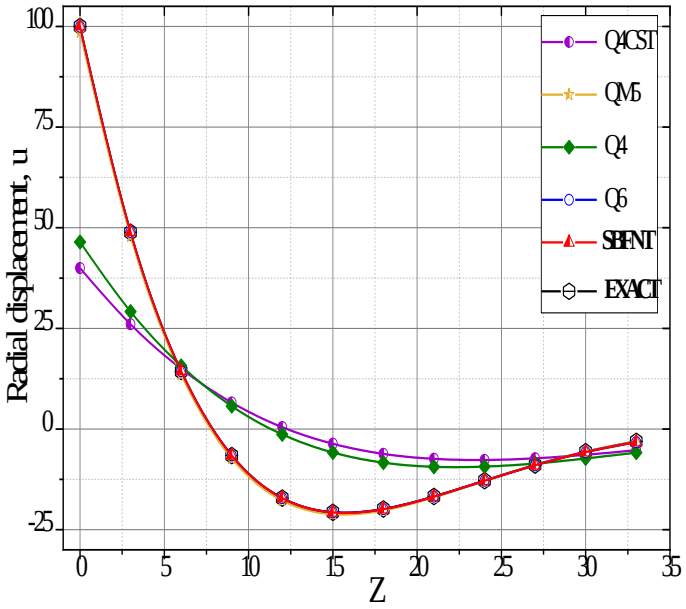

Figure 17. Radial displacements (u) for the axisymmetric cylindrical shell.

The obtained results reveal that the Q4 and Q4CST elements yield highly inaccurate values, indicating their inability to effectively capture bending phenomena. In contrast, the SBFNT, QM5, and Q6 elements demonstrate a high degree of accuracy in approximating the theoretical solution. The proposed element stands out for its exceptional performance in bending-dominated scenarios.

3.3 DYNAMIC NUMERICAL VALIDATION

3.3.1 EIGENVALUES OF A RECTANGULAR SOLID WITH LUMPED MASS

An elastic solid cantilever beam with a flexural rigidity of 1/12 and a Poisson's ratio of 0.3 is analyzed under plane strain conditions, as described in reference[50] and depicted in Figure 18. Two meshes are employed to evaluate the eigenvalues, with the results presented in Table 8.

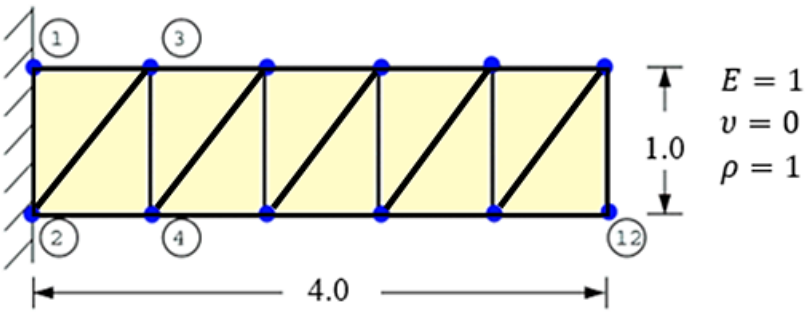

Figure 18. Geometrical and mesh representation of the cantilever beam.

Table 8. Eigenvalues of the cantilever beam

	Frequencies	Q4	Q8	SBE [41]	**SBFNT**
Mesh 3×1	ω_1	0.080	0.064	0.064	**0.070**
	ω_2	0.353	0.413	0.410	**0.376**
Mesh 5×1	ω_1	0.068	0.060	0.062	**0.066**
	ω_2	0.391	0.391	0.393	**0.3928**
Exact Solu[50]	$\omega_1 = 1.875^4 \times \frac{EI}{\rho AL^4}$		**0.063**		
	$\omega_2 = \pi/2L\sqrt{\frac{E}{\rho}}$		**0.393**		

For a coarse mesh (3×1), the SBFNT, SBE, and Q8 elements provide accurate approximations of the eigenvalues, approaching the exact theoretical solution. However, the Q4 element exhibits significant deviations from the exact solution. Refining the mesh to (1×5) leads to the convergence of the Q4 element's results towards the exact solution.

3.3.2 Forced vibration of a rectangular solid in-plane strain

The present benchmark study evaluates the performance of the developed element in a rectangular beam subjected to in-plane strain conditions, specifically examining its ability to analyze forced vibrations using the complex response method. The modeled results are compared against those obtained by Smith and Griffith[50] for the Q8 element, as well as the Q4, SBQ5, and SBRIE elements[40].

Figure 19 illustrates the geometrical dimensions and mechanical properties of the evaluated beam. The beam is subjected to a vertical harmonic force $F = \cos(\omega t)$, where the force-frequency is set to 0.3, the time step is $1/20$, the period is $2\pi/\omega$, and the damping ratio is 5%.

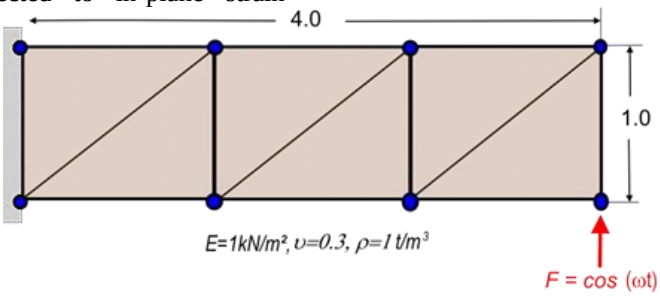

Figure 19. Geometrical and mesh presentation of the console beam subjected to forced vibration.

The displacements in respect to step time results are shown in figure 20. It is evident that the developed SBFNT element exhibits close agreement with the Q8 element.

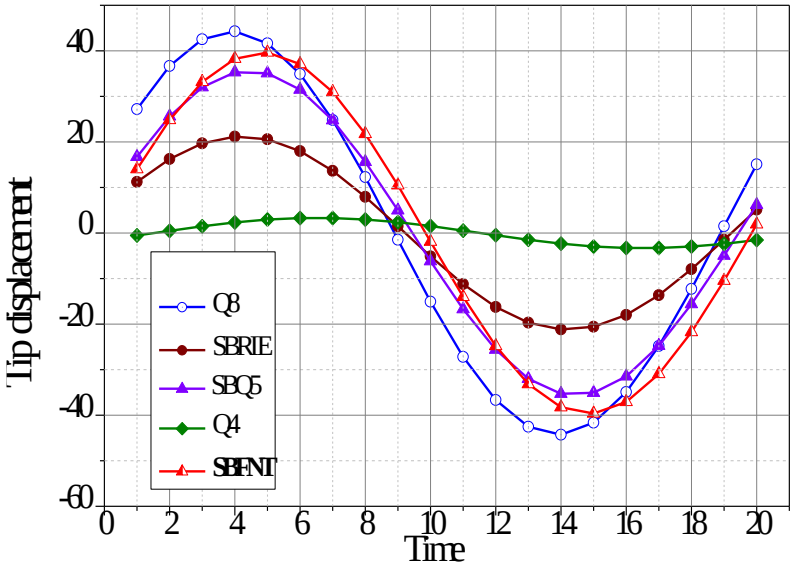

Figure 20. Displacement as a function of time for a console beam

3.4. CONCLUSION

This paper presents a novel strain-based triangular plane element. The incorporation of rigid body modes, constant strain, and compatibility conditions into the assumed strain field ensures and optimizes monotonic convergence to the solution.

The formulated element possesses four nodes with eleven degrees of freedom. The fourth node, located at the edge element's center, contributes two degrees of freedom (u, v). Static condensation eliminates this edge central node, resulting in a simple three-node element with three essential degrees of freedom (u, v, θ) at each corner node.

The SBFNT linear triangular element demonstrates satisfactory performance, mesh distortion insensitivity, and exceptional convergence characteristics across a variety of numerical examples. The proposed membrane element often achieves precision comparable to the second-order quadrilateral plane element Q8 in static and dynamic analyses of plane and axisymmetric structures.

Moreover, numerical results obtained using the proposed element yield consistent and improved outcomes in bending-dominated scenarios.

REFERENCES

1. D. G. Ashwell et A. B. Sabir, « A new cylindrical shell finite element based on simple independent strain functions », *International Journal of Mechanical Sciences*, vol. 14, nº 3, p. 171-183, 1972, doi: https://doi.org/10.1016/0020-7403(72)90074-4.
2. M. T. Belarbi et A. Charif, « Développement d'un nouvel élément hexaédrique simple basé sur le modèle en déformation pour l'étude des plaques minces et épaisses », *Revue Europeenne des Elements*, vol. 8, nº 2, p. 135-157, 1999.
3. M. Rezaiee-Pajand, N. Gharaei-Moghaddam, et M. Ramezani, « Strain-based plane element for fracture mechanics' problems », *Theoretical and Applied Fracture Mechanics*, vol. 108, p. 102569-102569, 2020.
4. M. Turner, R. Clough, H. Martin, et J. Topp, « Turner et al (1956) Stiffness and deflection analysis of comlex strucutres.pdf ».
5. I. C. Taig et R. I. Kerr, « Some problems in the discrete element representation of aircraft structures », *in: B.M. Fraeljs de Veubeke, ed., Matrix Methods of Structural Analysis (Pergamon Press, London, 1964)*.
6. W. Chen et Y. K. Cheung, « Axisymmetric solid elements by the generalized hybrid method », *Computers and Structures*, vol. 27, nº 6, p. 745-752, 1987.
7. K. Y. Sze, « On immunizing five-beta hybrid-stress element models from "trapezoidal locking" in practical analyses », *INTERNATIONAL JOURNAL FOR NUMERICAL METHODS IN ENGINEERING*, vol. 47, nº 4, p. 907-920, 2000.
8. K. Y. Sze A N et D. C. L. Chow, « AN INCOMPATIBLE ELEMENT FOR AXISYMMETRIC STRUCTURE AND ITS MODIFICATION BY HYBRID METHOD », *INTERNATIONAL JOURNAL FOR NUMERICAL METHODS IN ENGINEERING*, vol. 31, p. 385405-385405, 1991.
9. R. Ayad, « Eléments finis de plaque et coque en formulation mixte avec projection en cisaillement ». Compiègne, 1993.
10. F. Boussem et L. Belounar, « A Plate Bending Kirchhoff Element Based on Assumed Strain Functions », *JOURNAL OF SOLID MECHANICS*, vol. 12, nº 4, p. 935-952, 2020.
11. L. Belounar et K. Guerraiche, « A new strain-based brick element for plate bending », *Alexandria Engineering Journal*, vol. 53, nº 1, p. 95-105, 2014.
12. A. Kherfi, K. Guerraiche, et K. Zouggar, « Assessment of an Assumed Strain-based Quadrilateral Membrane Element », *Eng. Technol. Appl. Sci. Res.*, vol. 12, nº 5, p. 9302-9309, oct. 2022, doi: 10.48084/etasr.5182.
13. Z. H. Chen, Y. Guo, R. Jiang, et Q. Q. Guan, « Generalized conforming quadrilateral membrane element with vertex rotational freedom », *Chongqing Daxue Xuebao/Journal of Chongqing University*, vol. 32, nº 1, p. 31-36, 2009.
14. C. Wang, Z. Qi, X. Zhang, et P. Hu, « Quadrilateral 4-node quasi-conforming plane element with internal parameters », *Lixue Xuebao/Chinese Journal of Theoretical and Applied Mechanics*, vol. 46, nº 6, p. 971-976, 2014.
15. M. S. Djoudi et H. Bahai, « A shallow shell finite element for the linear and non-linear analysis of cylindrical shells », *Engineering Structures*, vol. 25, nº 6, p. 769-778, 2003.
16. M. Rezaiee-Pajand et M. Yaghoobi, « Formulating an effective generalized four-sided element », *European Journal of Mechanics, A/Solids*, vol. 36, p. 141-155, 2012.
17. D. G. Ashwell, A. B. Sabir, et T. M. Roberts, « Further studies in the application of curved finite elements to circular arches », *International Journal of Mechanical Sciences*, vol. 13, nº 6, p. 507-517, 1971.
18. J.-L. Batoz et G. Dhatt, « Modélisation des structures par éléments finis. Volume 1, Poutres et plaques », 1990.
19. A. Belounar, « Eléments finis membranaires et flexionnels à champ de déformation pour l'analyse des structures ». 2019.
20. [S. J. Fenves, N. Perrone, et A. R. Robinson, *Numerical and computer methods in structural mechanics*. Elsevier, 2014.
21. K. Guerraiche, « Eléments finis d élasticité plane et de volume basés sur l'approche en déformation ». 2014.
22. A. B. Sabir et M. S. Djoudi, « Shallow shell finite element for the large deflection

geometrically nonlinear analysis of shells and plates », *Thin-Walled Structures*, vol. 21, nº 3, p. 253-267, 1995, doi: https://doi.org/10.1016/0263-8231(94)00005-K.

23. D. Boutagouga, « A Review on Membrane Finite Elements with Drilling Degree of Freedom », *Archives of Computational Methods in Engineering 2020 28:4*, vol. 28, nº 4, p. 3049-3065, 2020, doi: 10.1007/S11831-020-09489-Z.
24. M. Rezaiee-Pajand, N. Gharaei-Moghaddam, et M. Ramezani, *Review of the strain-based formulation for analysis of plane structures*, vol. 11. in Iranian Journal of Numerical Analysis and Optimization, vol. 11. 2021.
25. A. Belounar, F. Boussem, M. N. Houhou, A. Tati, et L. Fortas, « Strain-based finite element formulation for the analysis of functionally graded plates », *Archive of Applied Mechanics 2022 92:7*, vol. 92, nº 7, p. 2061-2079, 2022, doi: 10.1007/S00419-022-02160-Y.
26. L. Belounar et M. Guenfoud, « A new rectangular finite element based on the strain approach for plate bending », *Thin-Walled Structures*, vol. 43, nº 1, p. 47-63, 2005.
27. F. Boussem, A. Belounar, et L. Belounar, « Assumed strain finite element for natural frequencies of bending plates », *World Journal of Engineering*, 2021.
28. S. CHICHOUNE et C. REBIAI, « ANALYSIS OF THIN PLATES IN BENDING BY NEW RECTANGULAR STRAIN BASED ELEMENT. », *Emirates Journal for Engineering Research*, vol. 28, nº 3, oct. 2023, [En ligne]. Disponible sur: https://scholarworks.uaeu.ac.ae/ejer/vol28/iss3/4
29. M. Bourezane, « An efficient strain based cylindrical shell finite element », 2017.
30. H. Guenfoud, M. Himeur, H. Ziou, et M. Guenfoud, « A consistent triangular thin flat shell finite element with drilling rotation based on the strain approach », *International Journal of Structural Engineering*, vol. 9, nº 3, p. 191-223, 2018.
31. A. Mousa, « Strain-Based Finite Element Analysis of Stiffened Cylindrical Shell Roof », *American Journal of Civil Engineering*, vol. 5, nº 4, p. 225-225, 2017.
32. C. Rebiai et L. Belounar, « A new strain based rectangular finite element with drilling rotation for linear and nonlinear analysis », *Archives of Civil and Mechanical Engineering*, vol. 13, nº 1, p. 72-81, 2013.
33. A. Belounar, F. Boussem, et A. Tati, « A novel C0 strain-based finite element for free vibration and buckling analyses of functionally graded plates », *Journal of Vibration Engineering & Technologies*, vol. 11, nº 1, p. 281-300, 2023.
34. C. Rebiai, « Finite element analysis of 2-D structures by new strain based triangular element », *Journal of Mechanics*, vol. 35, nº 3, p. 305-313, 2019.
35. C. Rebiai et L. Belounar, « An effective quadrilateral membrane finite element based on the strain approach », *Measurement: Journal of the International Measurement Confederation*, vol. 50, nº 1, p. 263-269, 2014.
36. R. D. Cook et H. Saunders, « Concepts and Applications of Finite Element Analysis (2nd Edition) », *Journal of Pressure Vessel Technology*, vol. 106, nº 1, p. 127-127, 1984.
37. M. Rezaiee-Pajand et M. Yaghoobi, « A robust triangular membrane element », *Latin American Journal of Solids and Structures*, vol. 11, p. 2648-2671, 2014, doi: 10.1590/S1679-78252014001400004.
38. M. T. BELARBI et M. BOUREZANE, « AN ASSUMED STRAIN BASED ON TRIANGULAR ELEMENT WITH DRILLING ROTATION », *Courrier du Savoir*, vol. 6, 2014, [En ligne]. Disponible sur: https://revues.univ-biskra.dz/index.php/cds/article/view/330
39. A. B. Sabir et S. A. B, « A rectangular and triangular plane elasticity element with drilling degrees of freedom », présenté à Chapter 9 in Proceeding of the 2nd International Conference on Variational Methods in Engineering, Southampton University, Springer-Verlag, Berlin, 1985, p. 17-25.
40. L. Bouzidi, L. Belounar, et K. Guerraiche, « Presentation of a new membrane strain-based finite element for static and dynamic analysis », *International Journal of Structural Engineering*, vol. 10, nº 1, p. 40-60, 2019.
41. C. Rebiai, N. Saidani, et E. Bahloul, « A New Finite Element Based on the Strain Approach for Linear and Dynamic Analysis », *Research Journal of Applied Sciences, Engineering and Technology*, vol. 11, nº 6, p. 639-644, 2015.
42. R. Winkler et D. Plakomytis, « A new shell finite element with drilling degrees of freedom and its relation to existing formulations », *ECCOMAS Congress 2016 - Proceedings of the 7th European Congress on Computational Methods in*

Applied Sciences and Engineering, vol. 2, nº September, p. 2803-2842, 2016.
43. L. Fortas, L. Belounar, et T. Merzouki, « Formulation of a new finite element based on assumed strains for membrane structures », *International Journal of Advanced Structural Engineering*, vol. 11, nº 1, p. 9-18, 2019, doi: 10.1007/s40091-019-00251-9.
44. R. H. Macneal et R. L. Harder, « A proposed standard set of problems to test finite element accuracy », *Finite Elements in Analysis and Design*, vol. 1, nº 1, p. 3-20, 1985.
45. P. G. Bergan et C. A. Felippa, « A triangular membrane element with rotational degrees of freedom », *Computer Methods in Applied Mechanics and Engineering*, vol. 50, nº 1, p. 25-69, 1985.
46. Y. K. Cheung, Y. X. Zhang, et W. J. Chen, « Refined nonconforming plane quadrilateral element », *Computers and Structures*, vol. 78, nº 5, p. 699-709, 2000.
47. W. Zouari, F. Hammadi, et R. Ayad, « Quadrilateral membrane finite elements with rotational DOFs for the analysis of geometrically linear and nonlinear plane problems », *Computers and Structures*, vol. 173, p. 139-149, 2016.
48. T. Goodier, « Theory of Elasticity. By Timoshenko and Goodier. 2nd Edition. 1951 Edition », *Journal of Elasticity*, vol. 49, p. 427-143, 1951.
49. S. P. Timoshenko, « Theory of Plates and Shells (McGraw-Hill Classic Textbook Reissue Series) ». 1964.
50. I. M. Smith, D. V. Griffiths, et L. Margetts, *Programming the Finite Element Method: Fifth Edition*. in Programming the Finite Element Method: Fifth Edition. 2015.

APPENDIX A

For calculation purpose the following matrices are given:

In plane stress

$$[D] = \frac{E}{1-\nu^2}\begin{bmatrix} 1 & \nu & 0 \\ \nu & 1 & 0 \\ 0 & 0 & \frac{1-\nu}{2} \end{bmatrix} \quad (A_1)$$

In plane strain

$$[D] = \frac{E}{(1+\nu).(1-2\nu)}\begin{bmatrix} 1-\nu & \nu & 0 \\ \nu & 1-\nu & 0 \\ 0 & 0 & \frac{1-2\nu}{2} \end{bmatrix} \quad (A_2)$$

Where [D] represents the elasticity matrix for plane stress and plane strain, respectively.